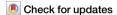
Published in partnership with the Sealy Institute for Vaccine Sciences



https://doi.org/10.1038/s41541-025-01130-z

Emulsion adjuvant-induced uric acid release modulates optimal immunogenicity by targeting dendritic cells and B cells



Sun Min Lee¹, Junghwa Lee¹, Dong-In Kim¹, Jonathan P. Avila², Helder Nakaya²³, Kihyuck Kwak⁴ & Eui Ho Kim¹,⁵⊠

Squalene-based emulsion (SE) adjuvants like MF59 and AS03 are used in protein subunit vaccines against influenza virus (e.g., Fluad, Pandemrix, Arepanrix) and SARS-CoV-2 (e.g., Covifenz, SKYCovione). We demonstrate the critical role of uric acid (UA), a damage-associated molecular pattern (DAMP), in triggering immunogenicity by SE adjuvants. In mice, SE adjuvants elevated DAMP levels in draining lymph nodes. Strikingly, inhibition of UA synthesis reduced vaccine-induced innate immunity, subsequently impairing optimal antibody and T cell responses. In vivo treatment with UA crystals elicited partial adjuvant effects. In vitro stimulation with UA crystals augmented the activation of dendritic cells (DCs) and B cells and altered multiple pathways in these cells, including inflammation and antigen presentation in DCs and cell proliferation in B cells. In an influenza vaccine model, UA contributed to protection against influenza viral infection. These results demonstrate the importance of DAMPs, specifically the versatile role of UA in the immunogenicity of SE adjuvants, by regulating DCs and B cells.

Vaccination is crucial for improving public health by preventing infectious diseases. Purified antigens, used in vaccines for their safety, often have reduced immunogenicity and require adjuvants to induce sufficient immune responses. Classical adjuvants include those based on pathogen-associated molecular pattern (PAMP) pathways, which stimulate imnate immune receptors to activate adaptive immune responses. Recently, the damage-associated molecular pattern (DAMP) pathway has emerged as a novel pathway. For instance, alum, a classical adjuvant, elicits adjuvant activity through the release of DNA, uric acid (UA), and ATP from dying cells, thus stimulating dendritic cell activation¹⁻⁴. Similarly, the saponin-based adjuvant component QS-21 stimulates innate cell recruitment and dendritic cell maturation through the local release of HMGB1 in draining lymph nodes (dLNs)⁵. Although advances have been made in identifying the danger signals involved in adjuvant effects, the underlying mechanisms of action are not comprehensively understood.

Squalene-based emulsion (SE) adjuvants are oil-in-water emulsions consisting of squalene, which are widely used in seasonal and pandemic influenza vaccines. MF59 (Novartis) and AS03 (GSK) are SE adjuvants included in licensed vaccines approved in Europe or USA. Despite the widespread use of MF59, its mechanism of action has not yet been fully

characterized. An in vitro study on human cells demonstrated that MF59 triggers the recruitment of monocytes and granulocytes to injection sites by inducing chemokine secretion and stimulating their differentiation into dendritic cells (DCs)⁶. In vivo studies further demonstrated the formation of an immunocompetent environment as a mechanism of action of MF59 in mice^{7,8}. Mechanistic studies have focused on immune cell activation and recruitment. The initial stages of these MF59 actions are suggested to be independent of TLRs and the Nlrp3 inflammasome9, similar to the mechanism of action of alum, a TLR-independent adjuvant. Recently, an in vivo study demonstrated that SE adjuvants flow to dLNs and that LNresident macrophages take up SE adjuvants to undergo cell death, which triggers antigen-specific CD8⁺ T cell responses¹⁰. They assumed that DAMPs might mediate cell death-induced immune responses based on observations of increased DAMP and pro-inflammatory cytokine levels in the serum after the administration of Addavax (AV)¹⁰. Here, they used Addavax (AV) for the in vivo experiments, as it has a similar formulation and comparable adjuvant effects to MF5910. MF59 has been reported to induce the release of ATP, promoting CD4+ T-cell and antibody responses¹¹. The role of UA is known with regard to the pathological aspect. Because the UA can activate the NLRP3 inflammasome, the hyperuricemia

¹Viral Immunology Laboratory, Institut Pasteur Korea, Seongnam, South Korea. ²Department of Clinical and Toxicological Analysis, School of Pharmaceutical Sciences, University of São Paulo, São Paulo, Brazil. ³Hospital Israelita Albert Einstein, São Paulo, Brazil. ⁴Department of Microbiology and Immunology, Yonsei University College of Medicine, Seoul, South Korea. ⁵Department of Advanced Drug discovery & development, University of Science and Technology (UST), Daejeon, South Korea. —e-mail: euiho.kim@ip-korea.org

npj Vaccines | (2025)10:72

1

that shows abnormally elevated serum UA level can be a causative factor in diseases such as gout¹². However, the mechanism of action of UA as a DAMP in vaccine response is poorly understood.

Based on this background, we hypothesized that UA is important for optimal vaccine responses to SE-adjuvanted vaccines. This study demonstrates that UA is essential for humoral and cellular responses to SE adjuvants through the activation of innate immunity. Furthermore, we describe the mechanisms of action of UA by addressing its direct effects on the functions and signaling of DCs and B cells.

Results

SE adjuvant induces the release of DAMPs and cytokines

First, we longitudinally tracked the early kinetics of DAMPs release in dLNs and serum following subcutaneous injection of the emulsion adjuvant. AV significantly increased the local concentrations of all three DAMP molecules (ATP, dsDNA, and UA) in dLNs (Fig. 1a). In particular, UA showed a gradual increase from the early hours until 48 h, although the systemic level of UA displayed an increasing tendency only at the early hours. The serum ATP and dsDNA levels remained largely unchanged. These results show that AV triggers the release of local DAMPs in the dLNs, and UA seemed to be dynamically affected among the tested DAMPs.

Next, we investigated whether inflammatory cytokines were induced by the emulsion adjuvants. To this end, we measured cytokine profiles in the dLNs and serum after AV administration. Although there were some kinetic differences of cytokine levels in between LN fluid and serum, there were rapid increases of IL-6 and MCP-1 at 6 h, while the peak level of IFN- γ was at 24 h post-administration. The peak levels of IL-27 and TNF- α were at 48 h or later after the vaccination with AV (Fig. 1b). The mildly affected or only locally increased cytokines are presented in Supplementary Fig. 1. The levels of IL-1 α , IFN- β , GM-CSF, and IL-10 were significantly increased only in dLNs, not in serum. Overall, the cytokine profiles showed an increase in pro-inflammatory cytokines in both the dLNs and serum.

Blocking UA abrogates humoral and cell-mediated immunity by SE adjuvant

Since all three DAMPs tested were released by the SE adjuvant, we were curious about the relative contribution of each DAMP molecule to SE adjuvant-mediated immunogenicity. Therefore, the release of ATP, dsDNA, and UA was temporarily monitored in vivo after the coadministration of DAMP blockers, including apyrase (ATPase), DNAse I, and uricase or febuxostat (a UA synthesis inhibitor). In vivo depletion of either ATP or dsDNA at the site of injection had no significant reducing effect on Ova-specific IgG levels, formation of germinal center (GC) B cells and follicular helper T ($T_{\rm FH}$) cells, or CD8 $^+$ T cell responses after Ova+AV vaccination (Supplementary Fig. 2).

Notably, the inhibition of UA by febuxostat significantly impaired Ovaspecific IgG responses (Fig. 2a). Consistent with the antibody-level data, the frequency of GC B cells was significantly decreased following febuxostat treatment (Fig. 2b and Supplementary Fig. 3a). Moreover, the generation of T_{FH} cells in the LNs was significantly reduced in the UA synthesis-inhibited mice (Fig. 2c and Supplementary Fig. 3a). These data indicate that UA contributes to AV-induced antibody responses by orchestrating GC B and T_{FH} cells. Next, we examined whether UA inhibition could attenuate T cell responses induced by the SE adjuvant. We observed that the frequency of activated CD4⁺ T cells (CD44⁺CD62L⁻CD4⁺ T cells) in the dLNs and spleen was decreased by UA inhibition (Fig. 2d and Supplementary Fig. 3a). In addition, ex vivo T cell stimulation and intracellular cytokine staining showed that the AV induced the increase of the IFN- γ -producing CD4 $^+$ T cell population, and that febuxostat treatment significantly inhibited those responses. Likewise, the frequencies of the activated CD8+ T cells (CD44+CD62L-CD8+ T cells) and Ova-specific CD8+ T cells (H2Kb-SIIN-FEKL tetramer (Tet)⁺CD44⁺CD62L⁻ CD8⁺ T cells) were reduced significantly by the inhibition of UA, as well, and the frequencies and the absolute numbers of IFN-y-producing CD8⁺ T cells were decreased by febuxostat (Fig. 2e and Supplementary Fig. 3b). In addition to the inhibition

of UA synthesis by febuxostat, the involvement of UA in AV-induced adaptive immune responses was evaluated using uricase, which degrades UA (Supplementary Fig. 4). UA depletion by uricase treatment consistently inhibited antibody responses, and the formation of GC B and $T_{\rm FH}$ cells and the activation of CD4 $^+$ and CD8 $^+$ T cells were moderately decreased. Taken together, UA plays a crucial role in the generation of optimal antibodies and T cell responses induced by the SE adjuvant.

UA contributes to the SE-induced innate immune responses

Based on the kinetics of UA release and the influence of UA on the adaptive immune responses to SE adjuvants, we explored the underlying mechanism of UA-mediated immunogenicity. As shown in Fig. 1b, we observed a potent induction of pro-inflammatory cytokines in the dLN fluid and serum upon AV administration. Following the in vivo prevention of UA synthesis by febuxostat treatment, local and systemic secretions of IL-6, IFN-γ, MCP-1, and TNF-α after AV injection were substantially decreased (Fig. 3a, b). The extent of reduction in other inflammatory cytokines by febuxostat was statistically insignificant (Supplementary Fig. 5). Next, we assessed the role of UA in the maturation of dendritic cells (DCs) at 24 h after immunization with AV alone or with febuxostat. Although the number of DC subsets was only significantly altered in resident DCs (CD11c⁺ MHCII⁺, rDCs) (Fig. 3c), the activation of total DCs (CD11c⁺), migratory DCs (CD11c^{int} MHCII^{hi}, mDCs), and rDCs in the dLNs was strongly stimulated by AV and significantly attenuated by febuxostat treatment (Fig. 3d). The rDCs were further analyzed for two major subsets: CD8⁺ DCs and CD11b⁺ DCs (Fig. 3e). The expression of the activation marker CD80 was increased by AV and decreased by febuxostat in all DC subsets (Fig. 3e). The increased frequency and number of neutrophils induced by AV in the dLN were decreased by febuxostat (Supplementary Fig. 6). The cell number of eosinophil was also increased by AV, and reduced by febuxostat. Collectively, these results show that UA plays an important role in triggering potent innate immune responses in dLNs following SE adjuvant administration.

Exogenous addition of UA demonstrates adjuvant effects

Given that UA is necessary for optimal vaccine-induced immune responses with the SE adjuvant, we next investigated whether exogenous administration of UA itself could enhance vaccine responses to antigens. We used UA crystals (monosodium urate, MSU) as a supplement to the protein antigen Ova in the absence of the SE adjuvant. Immunization with Ova and MSU induced a significantly higher antibody response in the serum than in mice immunized with Ova alone. (Fig. 4a). With regard to IgG subtypes, the stimulatory effect of MSU was prominent on Ova-specific IgG1 levels, and there was no significant change in IgG2b and IgG2c. Consistent with the antibody data, frequencies of GC B cells (median: MSU 5.485%, PBS 1.240%; FDR-adjusted P value, padj = 0.103) and TFH cells (median: MSU 3.665%, PBS 1.770%; padj < 0.01) were slightly augmented in the presence of MSU (Fig. 4b, c). MSU triggered notable increase of activated (CD44⁺CD62L⁻) CD4⁺ T cells, and there was mild inflation of IFN-γ-producing CD4⁺ T cells (cell no. median: MSU 1932 cells vs PBS 690 cells) in response to Ova peptide stimulation (Fig. 4d). The effects of MSU supplementation on CD8⁺ T cells were minimal, because either activated (CD44+CD62L-) CD8+T cells or Ovaspecific CD8+ T cells (Tet+CD44+CD62L) were marginally increased by MSU (Fig. 4e). These results demonstrate that MSU itself can effectively potentiate antigen-specific antibody responses but has a limited effect on CD8⁺ T cell responses.

UA directly targets DCs and potentiate their function

Based on the finding that UA facilitates innate and adaptive immune responses to SE adjuvants, we investigated the cellular targets of UA. We tested the effects of MSU on mouse immune cell subsets, including DCs, macrophages, B cells, and T cells, which may be involved in the SE adjuvant-induced immune responses. For this experiment, we prepared BMDCs or BMMs and isolated splenic T and B cells for ex vivo culture with MSU in the presence or absence of priming with low concentrations of LPS for BMDCs, BMMs, and B cells or with anti-CD3 and anti-CD28 antibodies for T cells. In

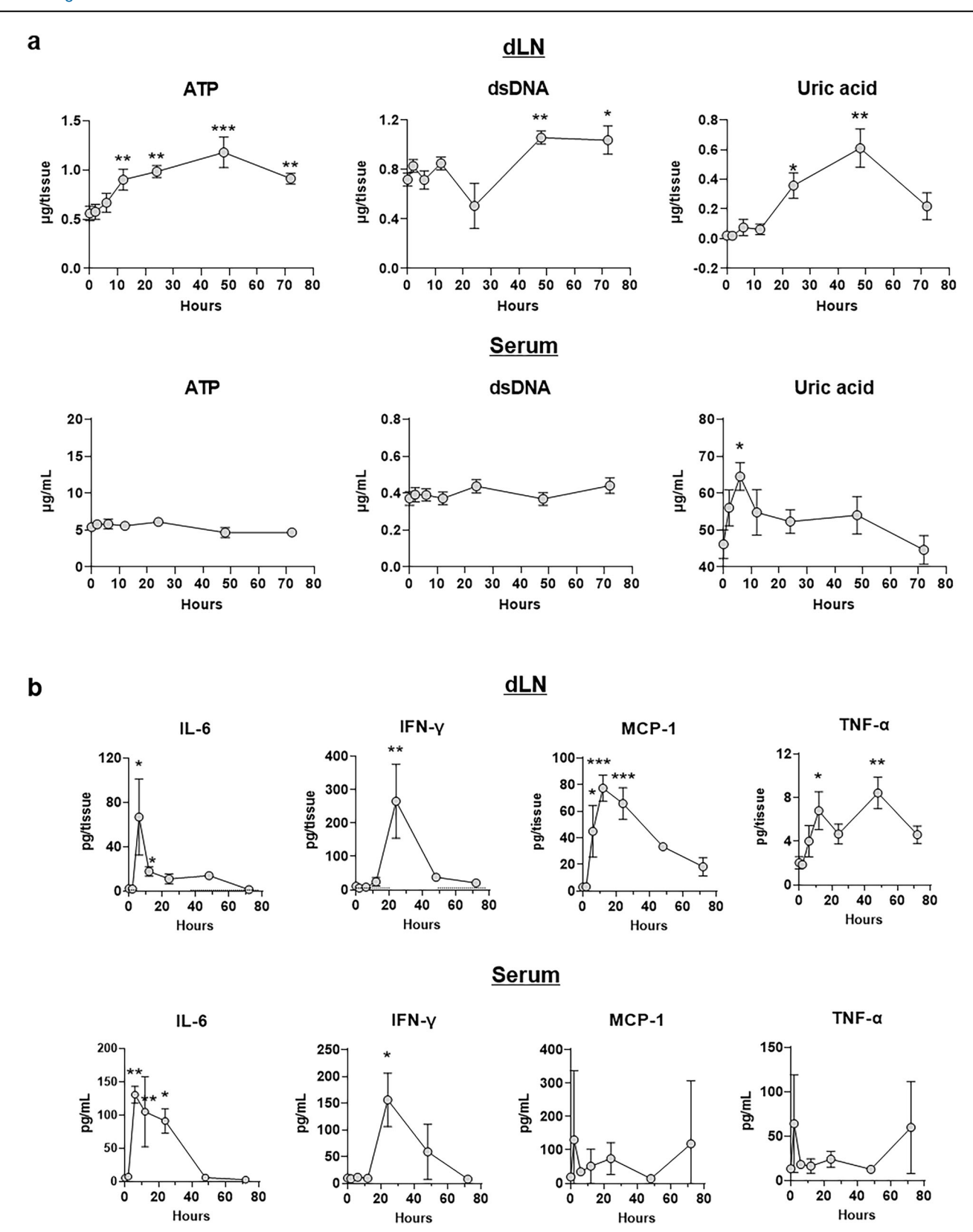
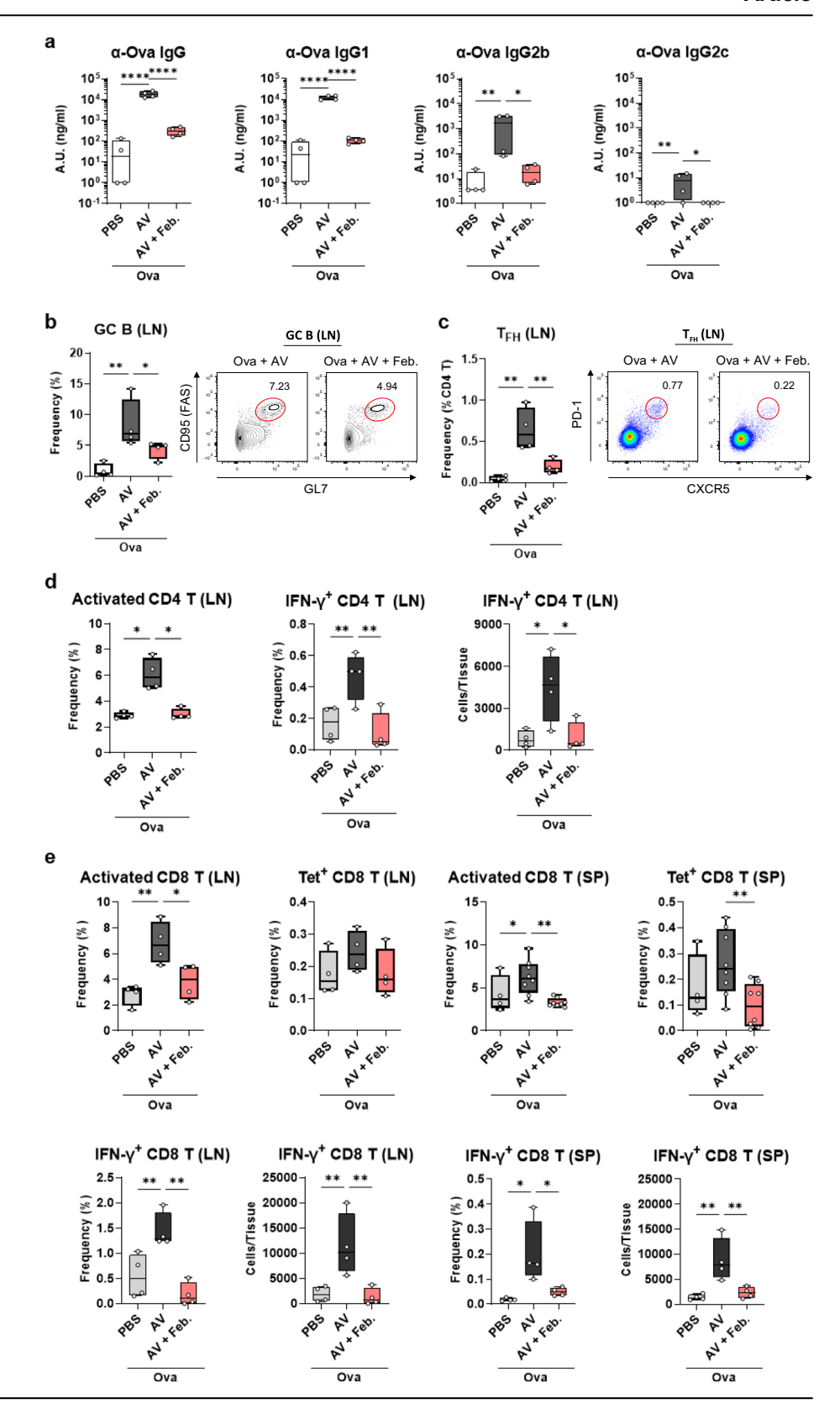


Fig. 1 | Time-dependent changes in DAMPs and cytokine levels during 72 h after administration of AV. WT B6 mice were subcutaneously injected with AV. DAMP and cytokine levels were measured in dLN and serum at 0, 2, 6, 12, 24, 48, and 72 h. Levels of (a) DAMPs (UA, ATP, and dsDNA) and (b) pro-inflammatory cytokines in dLN fluids and serum. *P < 0.05, **P < 0.01, ***P < 0.001 (in comparison with

0 h, by ANOVA or Kruskal-Wallis test). Data are pool of at least two independent experiments (mean and SEM). **a** dLN: n=7 mice at 0, 6, 12 h **and** n=4 at 2, 24, 48, 72 h). Serum: n=9 mice at each time-point. **b** dLN: n=6 mice at 0, 6, 12, 24 h and n=3 at 2, 48, 72 h. Serum: n=3 mice at each time-point.

Fig. 2 | Blocking UA abrogates humoral and cellmediated immunity by SE adjuvant. WT B6 mice were prime-boost immunized subcutaneously with AV ± febuxostat, with Ova antigen. a Levels of anti-Ova IgG, IgG1, IgG2b, and IgG2c. Frequency of (b) germinal center (GC) B cells and (c) follicular helper T (T_{FH}) cells in LNs. b, c Flow cytometry plots of GC B and T_{FH} cells are displayed. **d** Frequency of activated CD4+ T cells, frequency and cell number of IFN-γ+ CD4+ T cells in dLNs. e Frequencies of activated CD8+T cells and Tet+CD8T cells in dLNs and spleen, and frequency and cell number of IFN- γ^+ CD8⁺ T cells in dLNs and spleen. *P < 0.05, **P < 0.01, ****P < 0.0001 (ANOVA or Kruskal -Wallis test). Data are representative of at least two independent experiments (mean and SEM, n = 4 mice per group). Feb., febuxostat.



BMMs, MHC II and CD86 expression were slightly increased by MSU treatment in a dose-dependent manner. (Supplementary Fig. 7a). MSU had no direct stimulatory effect on T cells, which marginally reduced the expression of CD44 and CD69 (Supplementary Fig. 7b). In contrast, in DCs, the expression of MHC II, CD80, and CD86 was significantly increased by MSU in a dose-dependent manner (Fig. 5a).

To understand how MSU promotes DC activation, we analyzed the transcriptional profiles of BMDCs three hours after MSU stimulation. According to RNA sequencing data, overall 737 genes were up-regulated, 648 genes were down-regulated, and 15,725 genes were unperturbed (Fig. 5b). Annotation of the genes into pathway databases indicated the pathways upregulated by MSU in DCs, including TNF-α signaling via NF-κB,

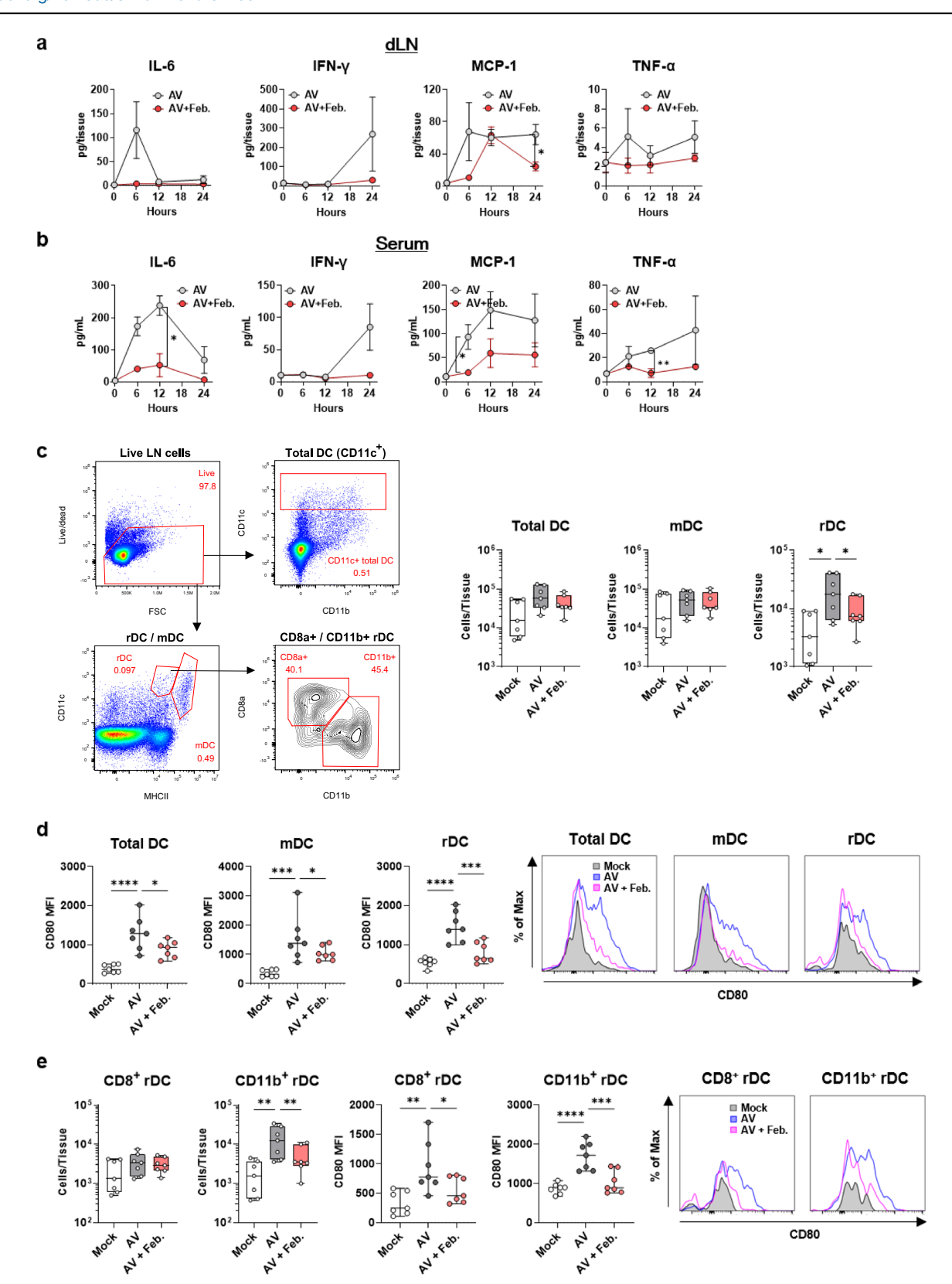


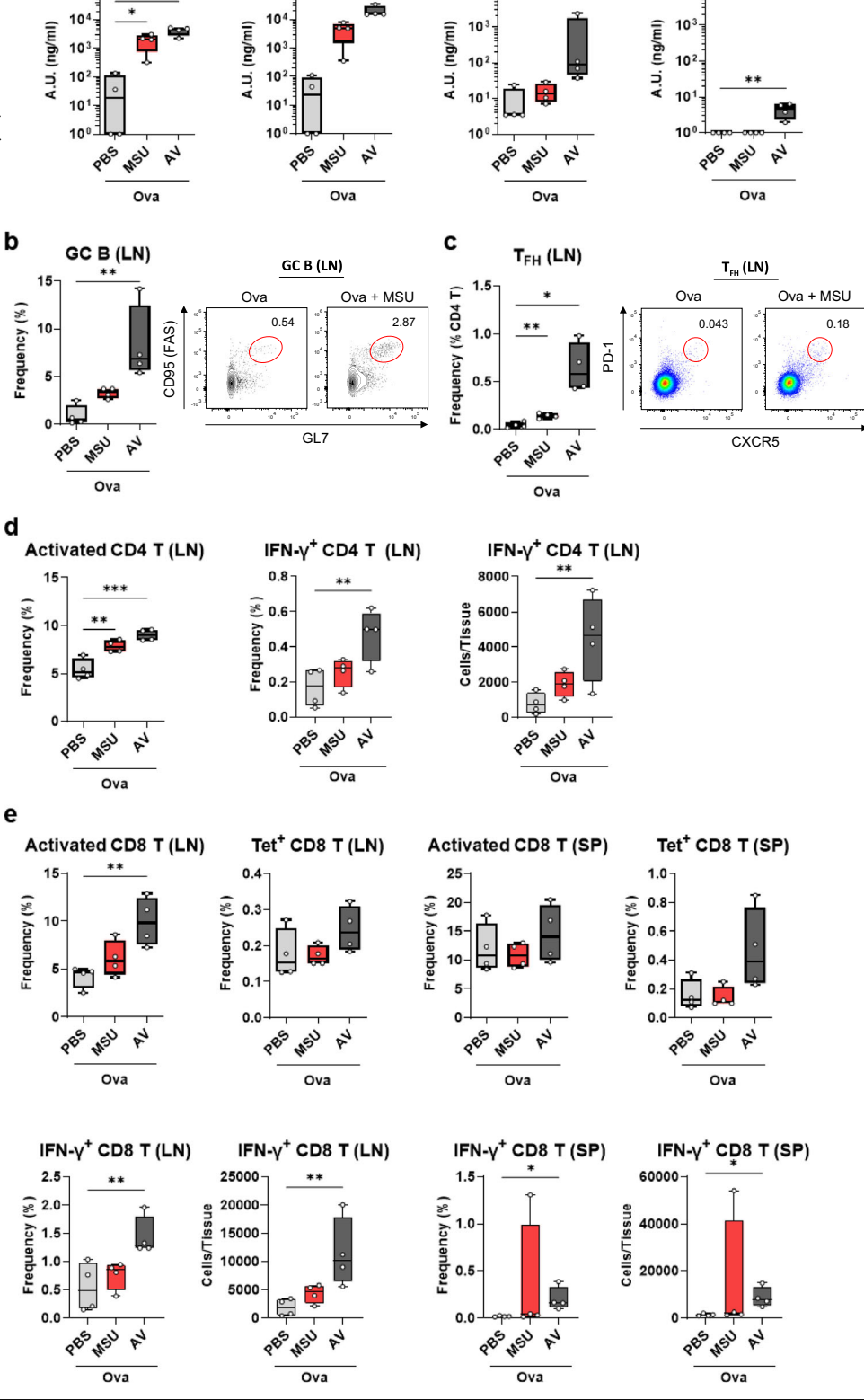
Fig. 3 | Perturbation of UA suppresses the innate immunity during vaccination. WT B6 mice were immunized subcutaneously with AV \pm febuxostat. dLN fluid and serum were obtained at 6, 12, and 24 h after immunization to measure proinflammatory cytokine levels in (a) dLN fluid and (b) serum. $\mathbf{c}-\mathbf{e}$ At 24 h postimmunization, the dLN cells were analyzed by flow cytometry. \mathbf{c} Flow cytometry plots show the gating of total DCs, migratory DCs (mDCs), and resident DCs (rDCs) in live LN cells. Total DCs were gated on CD11c $^+$ cells. rDCs and mDCs were characterized by gating on CD11c $^+$ MHCII $^{\mathrm{lo}}$ cells (rDCs) and CD11c $^+$ MHCII $^{\mathrm{lo}}$

(mDCs). The rDCs were further analyzed in CD8⁺ rDCs and CD11b⁺ rDCs. Cell number per LN tissue of (c) total DCs, mDCs, rDCs, (e) CD8⁺ rDCs and CD11b⁺ rDCs. CD80 MFI of (d) total DCs, mDCs, rDCs, (e) CD8⁺ rDCs and CD11b⁺ rDCs. d, e Histograms show CD80 expression levels in each DC subsets. $\mathbf{a}-\mathbf{b}$ Data are representative of two independent experiments (mean and SEM, n = 3 mice per group at each time-point). *P < 0.05, **P < 0.01 (t-test). $\mathbf{c}-\mathbf{e}$ Data are pool of two independent experiments (mean and SEM, n = 7 mice per group). *P < 0.05, **P < 0.01, ***P < 0.001, ****P < 0.001, *****P < 0.001, ****P < 0.001

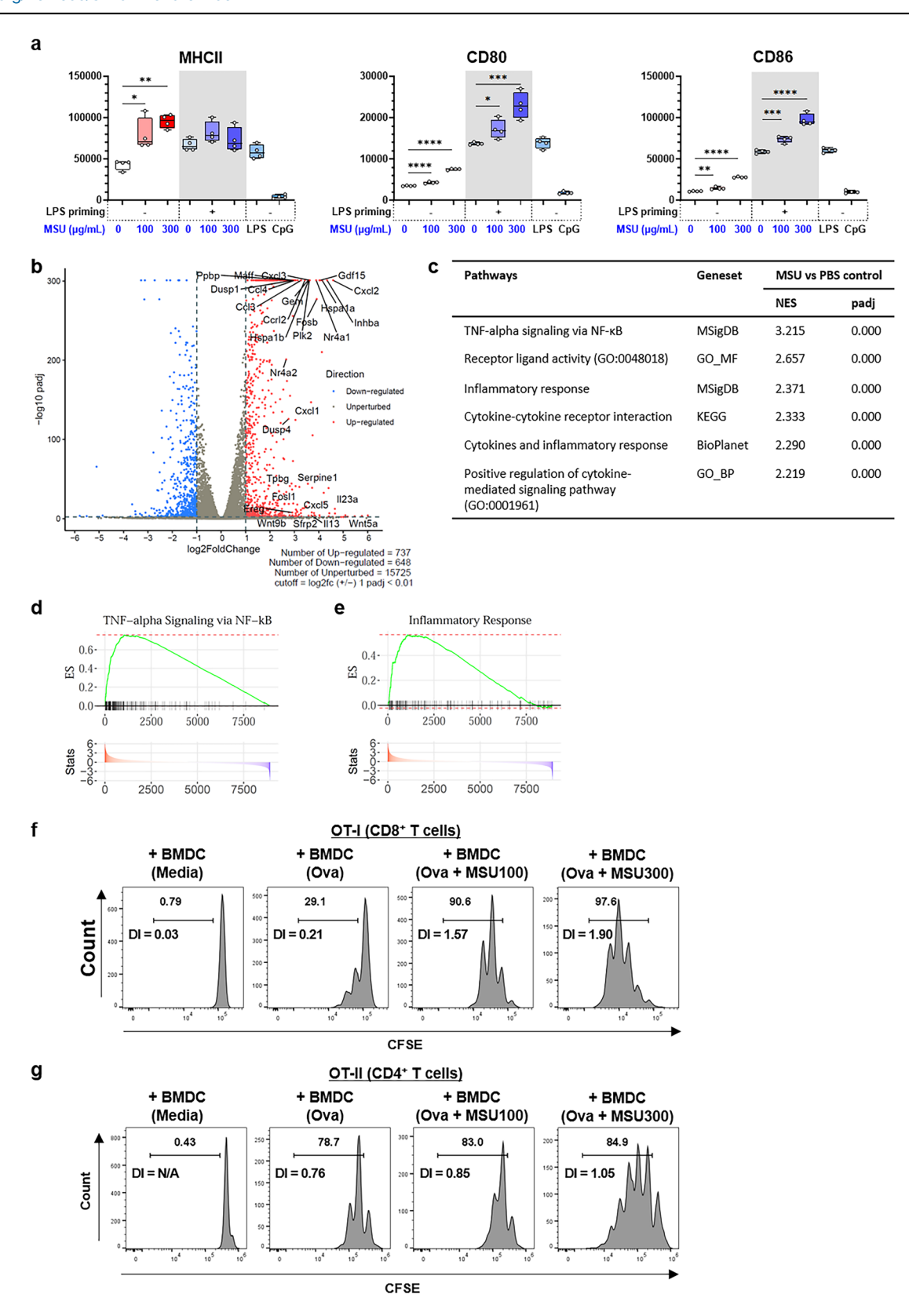
α-Ova IgG2c

104

a Fig. 4 | In vivo treatment of UA crystals with α-Ova IgG α-Ova IgG1 α-Ova IgG2b antigen enhances adaptive immune responses. 10 10 10 WT B6 mice were immunized subcutaneously with MSU or AV, with Ova antigen. Adaptive immune A.U. (ng/ml) A.U. (ng/ml) A.U. (ng/ml) 10 10 responses were analyzed at day 7 post-boosting. 102 a Levels of anti-Ova IgG, IgG1, IgG2b, and IgG2c in 10 10 serum. Frequency of (b) germinal center B cells and 101 10 (c) follicular helper T cells in dLNs. d Frequency of activated CD4+T cells, frequency and cell number of IFN-γ+ CD4+ T cells in dLNs. e Frequencies of activated CD8+T and Tet+CD8+T cells in dLNs and Ova Ova spleen, and frequency and cell number of IFN-γ+ CD8⁺ T cells in dLNs and spleen. Data are repre-C GC B (LN) sentative of at least two independent experiments GC B (LN) (mean and SEM, n = 4 mice per group). *P < 0.05, Ova + MSU (% CD4 T) **P < 0.01, ***P < 0.001 (ANOVA or Kruskal-Frequency (%) 0.54 10 CD95 (FAS) Wallis test). MSU, monosodium urate. 1.0 Frequency 0.5 0.0 GL7 Ova d Activated CD4 T (LN) IFN-y+ CD4 T (LN) Frequency (%) 5.0 4.0 5.0 6000 4000 2000 Frequency (%)



receptor ligand activity, inflammatory response, and cytokine responses (Fig. 5c). First, the 'TNF-alpha signaling via NF-κB' pathway genes were upregulated by MSU in BMDCs, with the highest NES among the pathways (padj < 0.001) (Fig. 5d). It is known that antigen presentation by DCs is dependent on NF-κB signaling pathway¹³. Therefore, the upregulation of this pathway in our data implied the stimulation of NF-kB pathway in the DC activation by MSU. Second, the 'inflammatory response' pathway showed an increase by MSU in BMDCs (padj < 0.001) (Fig. 5e). The inflammatory responses of the DCs were also evidenced by the increase of other relevant pathways: 'receptor ligand activity', 'inflammatory response', 'cytokine-cytokine receptor interaction', 'cytokines and inflammatory response', and 'positive regulation of cytokine-mediated signaling pathway'



(all padj < 0.001) (Fig. 5c). Among the leading-edge genes of the 'inflammatory response' pathway, Inhba increased the most (log₂ fold change, log2FC = 4.342) by MSU in BMDCs (Supplementary Table 1). Inhba is a gene encoding inhibin A, a member of the TGF β family, which is known to be essential for DC maturation, evidenced by the decrease of MHCII, CD80, and CD86 in BMDCs from inhibin knockout mice¹⁴. Among the leading

edge genes in the 'receptor ligand activity' pathway, Wnt5a, a member of Wnt signaling pathway, was the most increased gene. Wnt5a contributes to antigen processing/presentation and CD8⁺ T-cell activation¹⁵. Moreover, our gene profile showed an increased expression of Ccr7 (log2FC = 1.111), which is crucial for the migration of DCs to the LNs^{16–18}. Taken together, the pathway and DEG analyses revealed transcriptomic changes in MSU-

Fig. 5 | **UA crystals trigger the activation of BMDCs. a** BMDCs were treated with MSU and analyzed with flow cytometry at 24 h. MFIs of activation markers MHCII, CD86, and CD80. **b**−**e** BMDCs were stimulated with MSU for 3 h ex vivo. **b** Volcano plot of bulk mRNA sequencing of BMDCs (MSU vs PBS control) with cut-off at | log2FC | > 1 and padj < 0.01. Gene names of the most highly increased genes (based on log2FC) of the relevant pathways shown in (**c**) are marked on the volcano plots. **c** NES and padj (MSU vs PBS control) of pathways increased in MSU-treated BMDCs. Pathways relevant to the vaccine responses are described. FGSEA plots of (**d**) inflammatory responses and (**e**) TNF-alpha signaling. Histograms of CFSE-

stained (f) OT-I (CD8⁺ T) and (g) OT-II (CD4⁺ T) cells show the increased proliferation of the OT-I (CD8⁺ T) or OT-II (CD4⁺ T) cells after co-culturing with MSU-stimulated BMDCs. a Data are representative of two independent experiments (n = 4 independent biological replicates). Box extends from 25th to 75th percentiles, and all points are shown with median, min and max. *P < 0.05, **P < 0.01, ****P < 0.0001 (ANOVA or Kruskal-Wallis test). **b**—**e** n = 3 independent biological replicates. **f**, **g** Percentage of divided cells are shown as numbers. Data are representative of two independent experiments (n = 3 independent biological replicates). NES, normalized enrichment score; DI, division index.

treated BMDCs toward DC maturation, effective antigen processing/presentation, and migration.

To predict the cellular receptors of MSU through the RNA sequencing data, we further investigated the upstream receptors of the activated genes using the ShinyGo analysis tool (http://bioinformatics.sdstate.edu/go80/)¹⁹. The activated pathways in MSU-stimulated BMDCs were mediated by various receptors including IL-1R, CD14, IL-17RA, TLR1, TLR2, EGFR, IFNGR, and GPCR (Supplementary Table 2). Among the MSU-stimulated pathways, there was an upregulation of the NLR signaling pathway in BMDCs with the increased expression of NLRP3 inflammasome components (NLRP3 and ASC) and IL-1β (Supplementary Table 2). According to the KEGG database, an upstream receptor of NLR signaling is G proteincoupled receptor (GPCR), with orthologs K04612 (calcium-sensing receptor) and K04622 (GPCR6A). Notably, our data showed increased expression of the GPCR and its subsequent NLRP3 inflammasome components (NLRP3 and ASC), and downstream products (pro-IL-1β and IL-1β) in the KEGG pathway (Supplementary Fig. 8). According to functional enrichment analysis, the GPCR signaling pathways were upregulated with MSU in BMDCs (Supplementary Table 3). Specifically, the *Gprc5a* expression level commonly increased by MSU both in BMDC and B cells (Supplementary Table 4).

We further conducted a functional verification to determine whether MSU-treated DCs exerted a superior capacity for antigen presentation. BMDCs were stimulated with Ova in the presence or absence of MSU, followed by co-culture with naïve T cells obtained from OT-I or OT-II TCR transgenic mice for three days. Both OT-I (CD8⁺ T) and OT-II (CD4⁺ T) cells showed increased proliferation in MSU-treated BMDCs in a dose-dependent manner (Fig. 5f, g). Together, these data imply that UA directly triggers DC activation, leading to an enhanced T cell response following SE-adjuvanted vaccination.

UA directly stimulates B cell activation

Next, we examined whether UA crystals directly affected B cells by assessing their activation status in vitro in the presence of MSU. MSU treatment increased the expression levels of MHC II, CD69, and CD86 in a dose-dependent manner (Fig. 6a).

To determine the mechanism underlying B-cell activation by MSU, we analyzed the mRNA profile 3 h after stimulation with MSU. In the B cell transcriptional analysis data, 218 genes were up-regulated, 17 genes were down-regulated, and 11610 genes were unperturbed (Fig. 6b). Annotation of all genes showed that pathways were altered by MSU in B cells, including the IL-2 signaling pathway, positive regulation of cell population proliferation, and cellular response to cytokine stimulus. (Fig. 6c-f). Pathway analysis results indicated alterations in gene expression related to B cell functions in vaccine responses. First, IL-2 signaling pathway was activated by MSU in the splenic B cells (padj = 0.004) (Fig. 6d). Second, 'positive regulation of cell population proliferation' pathway significantly increased by the MSU in B cells (padj = 0.011) (Fig. 6e). This is notable given that B-cell proliferation and differentiation into effector B cells are important processes for effective B cell response and antibody production. It is reasonable that the RNA sequencing data only showed proliferation, considering that the B cells were in the early phase of activation. The leading edges of the upregulated pathways included genes related to B cell functions during vaccine responses, such as Il2, Myc, Il10, and Irf4 (Supplementary Table 5). In particular, *Il2* is upregulated in plasma cells and is well understood for its ability to stimulate B cell activation and proliferation²⁰. *Myc* regulates cell proliferation and differentiation²¹. *Il10* increase gradually in marginal zone B cells, germinal center B cells, and plasma cells²². Autocrine IL-10 is involved in B cell differentiation into plasmablasts²³. *Irf4* is a transcription factor essential for the differentiation of T and B cells. It is highly expressed in plasma cells and is involved in germinal center responses and plasma cell differentiation^{22,24}. Among all of the DEGs, the most highly upregulated gene was *Ifi202b* (log2FC = 9.820, padj < 0.001) (Fig. 6b). *Ifi202b* is an IFN-inducible gene that is highly expressed in plasma and marginal zone B cells²². Considering that IFNs enhance B cell recruitment, upregulation of *Ifi202b* may indicate an indirect pathway of B cell response to MSU^{25,26}. Overall, the transcriptional data indicate that MSU facilitates B cell and antibody responses by stimulating the proliferation and plasma cell differentiation of B cells.

The upstream receptors of the upregulated pathways in B cells in the presence of MSU were IL-1R, IL-2R, and TNFR2 (Supplementary Table 2). Consistent with the increase in BMDCs, the GPCR signaling pathways were upregulated in splenic B cells (Supplementary Table 3), with the increase of *Gprc5a* expression (Supplementary Table 4).

UA is critical for the protective immunity in SE-adjuvanted influenza vaccine

Finally, we aimed to confirm the essential role of UA in the protective efficacy of the SE-adjuvanted influenza vaccine. Therefore, mice were vaccinated and subsequently challenged with a lethal dose of live influenza virus. For this purpose, recombinant HA protein from the A/PR8/ 1934(H1N1) virus was utilized as a vaccine antigen, and different additives such as MSU, AV, and AV+febuxostat were used. We first tested the protective efficacy of a single-dose vaccine in mice. Three weeks after immunization, anti-HA IgG levels were not detectable in the HA-only group, but MSU supplementation enhanced the IgG responses (Fig. 7a). The AV adjuvant generated the highest IgG response against HA, and blocking UA significantly attenuated the antibody levels. We also determined the titer of neutralizing antibodies using plaque reduction neutralization tests (PRNT) (Fig. 7a). The single dose of HA with MSU or AV supplementation slightly induced the production of neutralizing antibodies, whereas the titer was not detectable in the HA-only group at this time point. Blocking UA with febuxostat seem to suppress the normal production of neutralizing antibodies. The mice were infected with a lethal dose of live influenza virus. As a result, only HA + AV group displayed attenuated weight loss and 100% survival (Fig. 7b, c). Notably, the febuxostat treatment largely negated the protective effects of AV on survival (100% survival in AV vs. 20% survival in AV+febuxostat; Fig. 7b, c). In contrast, prime-boost vaccination of mice under the same conditions narrowed the gaps in HA-specific IgG levels and survival between groups (Fig. 7d, f). Nevertheless, viral challenge after prime-boost immunization demonstrated the enhancement of protective capacity by MSU supplementation of the HA antigen, at least in part (Fig. 7d-f). In addition, neutralizing antibody titers were increased by MSU supplementation during the HA vaccination, and febuxostat treatment consistently inhibited AV-induced neutralizing antibody production (Fig. 7d). Collectively, these data suggest the crucial role of UA in providing protective immunity against influenza vaccination by modulating adaptive immune responses.

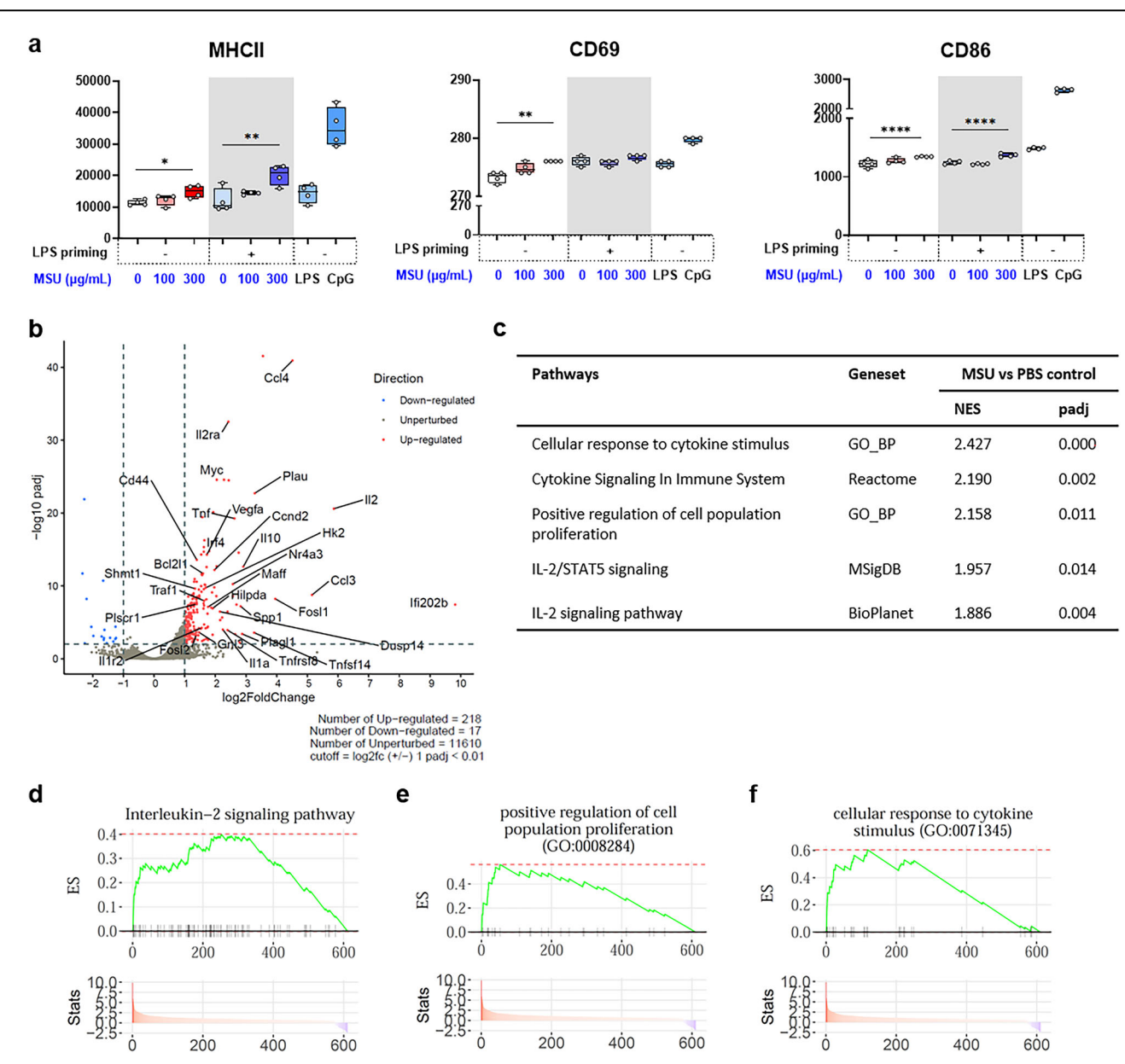


Fig. 6 | **UA crystals stimulate the activation of B cells. a** Splenic B cells were stimulated with MSU, and analyzed with flow cytometry at 24 h. MFIs of activation markers MHCII, CD86, and CD69. $\mathbf{b}-\mathbf{f}$ Splenic B cells were treated with MSU for 3 h ex vivo. \mathbf{b} Volcano plot of bulk mRNA sequencing of B cells (MSU vs PBS control) with cut-off at $|\log_2 FC| > 1$ and padj < 0.01. Gene names of the most highly increased genes (based on log2FC) of relevant pathways shown in (\mathbf{c}) are marked on the volcano plots. \mathbf{c} NES and padj (MSU vs PBS control) of pathways increased in MSU-treated B cells. Relevant pathways are shown. FGSEA plots of (\mathbf{d})

'interleukin-2 signaling' and (e) 'positive regulation of cell population proliferation' and (f) 'cellular response to cytokine stimulus'. a Data are representative of two independent experiments (n = 4 independent biological replicates). Box extends from 25th to 75th percentiles, and all points are shown with median, min and max. *P < 0.05, **P < 0.01, ****P < 0.001 (ANOVA or Kruskal-Wallis test). $\mathbf{b} - \mathbf{f}$ PBS control (n = 3 independent biological replicates), MSU (n = 2 independent biological replicates). NES, normalized enrichment score.

Discussion

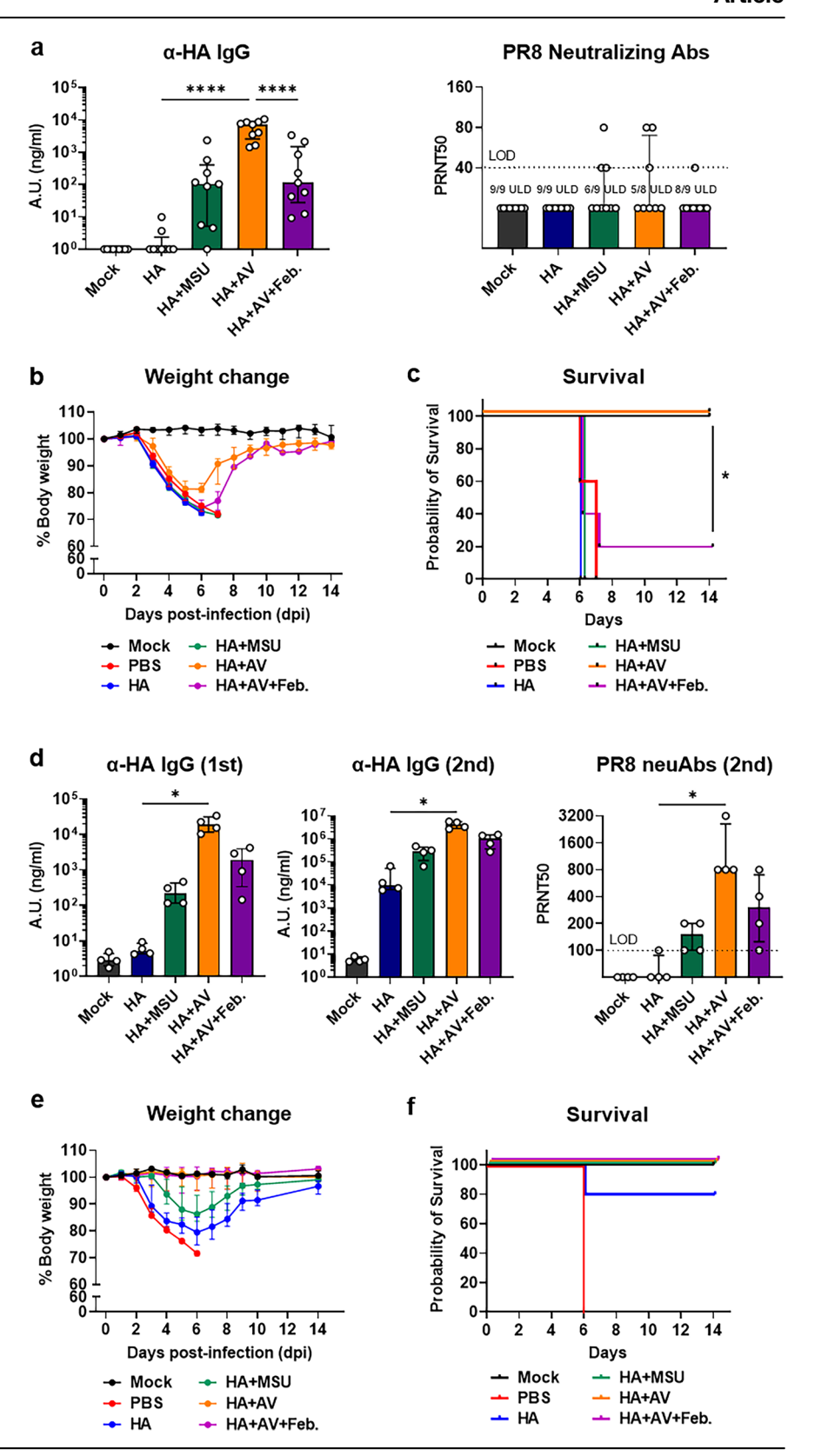
In this study, we have demonstrated the essential role of UA in the optimal immunogenicity of SE adjuvant-containing vaccines and its direct effect on specific immune cells. This allowed us to understand the underlying mechanism of SE adjuvant action and to suggest the possibility of UA-mediated pathways as novel targets for enhancing immunity.

According to a previous study, ATP is transiently released from muscles during the 30 min period after intramuscular administration of MF59, and the generated ATP shapes the humoral immune response to MF59¹¹. In addition to ATP, an earlier study identified the release of UA as a danger signal that triggered DC activation in mice²⁷. Notably, our data clearly showed that the SE adjuvant triggered the release of UA in the context of vaccination and promoted the optimal induction of antibody and

T cell responses. At the same time, it is important to note that the recovery of transiently elevated DAMPs to basal levels was seen in our data, since consistently elevated UA can lead to chronic inflammation, which can be pathogenic¹². Regarding this concern, we also showed that after short period of time (6–72 h), pro-inflammatory cytokine levels returned to normal levels. In addition, IL-27 is a pleiotropic cytokine with both immune-stimulatory and anti-inflammatory functions. A recent study reported that IL-27 secreted by myeloid cells acts on CD8 T cells to sustain their expansion²⁸. In contrast, given that the IL-27 can also function as a regulatory cytokine²⁹, we suppose that the IL-27 at 48 h in LNs may regulate the early inflammatory responses to suppress excessive inflammation. SE adjuvants elicit immunogenicity through the formation of immunocompetent environment^{7,8}. Administration of SE-adjuvant AV recruits

Fig. 7 | UA crystals protects from lethal viral infection through enhancing vaccine effects.

BALB/c mice were immunized with (a-c) single or $(\mathbf{d} - \mathbf{f})$ double (prime-boost) doses of 0.1 µg HA with MSU, AV, or AV + febuxostat. $\mathbf{d} - \mathbf{f}$ Boosting vaccination was performed at day 21 after the primary vaccination. The mice were infected with PR8 at $(\mathbf{a}-\mathbf{c})$ day 28 after the primary or $(\mathbf{d}-\mathbf{f})$ day 21 after the boosting vaccination. Monitored daily for body weight decrease and survival for 2 weeks. Anti-HA IgG levels and PR8 neutralizing antibody titers in serum at (a) day 25 after vaccination, or (d) at day1 (as a primary response) and 15 post-boosting (as a secondary response). b, e Changes in body weight of mice after challenge with a lethal dose of PR8. c, f Survival rate of the mice to PR8 infection. Data are representative of two independent experiments (median with interquartile range). \mathbf{a} n = 9 mice per group. \mathbf{b} , \mathbf{c} n = 5 mice per group except HA group (n = 4). **d** n = 4 mice per group. **e**, **f** n = 5 mice per group except PBS group (n = 3). \mathbf{a} , $\mathbf{d} * P < 0.05$, ***P < 0.001, ****P < 0.0001 (ANOVA or Kruskal-Wallis test). c *P < 0.05 (log-rank test). Feb., febuxostat.



immune cells including neutrophils, and stimulates the activation of DCs in dLNs¹⁰. This finding is consistent with the results of the present study. Furthermore, we propose that UA release by the SE adjuvant is essential for this process, based on the reduced frequency of neutrophils and low activation of DCs in dLNs through depletion of UA during immunization. Neutrophils are known to contribute to DC activation through the release of

cytokines and chemokines, including TNF 6,30 . Consistent with previous findings, our cytokine data support the idea that the elimination of UA impairs the secretion of pro-inflammatory cytokines, including TNF, both in local and systemic circumstances. The local increase of IL-1 α , IFN- β , and GM-CSF in dLNs indicate the recruitment of innate immune cells by AV. Our data showed that AV induced the activation of DC subsets, including

mDCs, CD8⁺ rDCs, and CD11b⁺ rDCs, which was inhibited by UA depletion in vivo. This suggests that UA is required for proper maturation of DC subsets for CD4⁺ and CD8⁺ T cell stimulation. UA depletion also inhibited eosinophil recruitment to dLNs. Interestingly, it has been previously demonstrated that human eosinophils can recognize danger signals from UA crystals to elicit pro-inflammatory cytokine production via autocrine ATP production³¹. As a mechanism of alum, it has been reported that eosinophils may be necessary for vaccine responses considering that they mediate alum-elicited early B cell priming and IgM generation³². Further studies are required to understand the exact role of eosinophils in the immunogenicity of SE adjuvants. Overall, our results indicate that UA contributes to the formation of an immunocompetent environment during the early phase of immunization with SE adjuvants.

The present study showed that blocking UA substantially inhibited the CD4⁺ and CD8⁺ T cell responses to AV. In contrast, exogenous MSU triggered a CD4⁺ T cell response without significantly affecting CD8⁺ T cell activation. The minimal effect on CD8⁺ T cells by MSU in our study is likely because MSU alone may not be sufficient to mimic the complicated immunocompetent conditions generated by the SE adjuvant. According to a previous study, CD8⁺ T cell responses to the SE adjuvant require uptake of the adjuvants by LN-resident macrophages¹⁰. The SE adjuvant induces RIPK3-dependent cell death in medullary macrophages, which activates Batf3⁺ DCs that are responsible for antigen cross-presentation to CD8⁺ T cells¹⁰. Considering that cell death induces the release of DAMPs other than UA, it is plausible that administration of MSU alone may not be sufficient to stimulate these cellular pathways. Cytokines and other DAMPs may be involved along with UA for the activation of Batf3⁺ DCs, which is necessary for sufficient CD8+ T cell activation. Indeed, HMGB1 released from dying tumor cells, which is recognized by TLR4 in DCs, is crucial for antigen processing for cross-presentation and for triggering the activity of cytotoxic CD8⁺ T cells^{33,34}. In addition, the delivery of MSU to the LNs can be limited because of its crystal form. This is important, because the SE adjuvant induces cell death in LN-resident cells¹⁰. Hence, in situ UA generation via cell death by AV is essential for the immunogenicity of AV; however, the administration of exogenous UA crystals may not be able to fully mimic the physiological environment.

Regarding the cellular sensing of MSU, an early suggested mechanism is lipid-based interaction independent of receptor signaling³⁵. On the other hand, there have been suggestions for UA receptors, such as urate anion transporter 1 (URAT1) and Clec12a as UA crystal receptors that can trigger pro-inflammatory responses in human macrophages³⁶ or IFN-I responses in BMDCs^{37,38}, respectively. The murine Naip1-Nlrp3 inflammasome has also been predicted to be a sensor of UA in mice³⁹. Among upregulated receptors in our RNA sequencing data, we focused on GPCR as a possible MSU sensor because it was discovered as an upstream receptor of a known signaling outcome of MSU (NLRP3 inflammasome activation). Similarly, a previous report showed that IL-1β production by MSU in BMM depends on purinergic receptor P2YRs, a family of GPCRs4. The functional enrichment analysis showed the activation of GPCR signaling in BMDCs and B cells. Moreover, MSU stimulation in BMDCs increased the expression levels of the GPCR ortholog and the downstream components within the NLR signaling pathway. Therefore, the present study demonstrates multiple receptors and pathways responsive to MSU in DCs and B cells and proposes that GPCRs may need to be studied for its ability to recognize MSU.

The main consequence of MSU stimulation in immune cells is activation of the NLRP3 inflammasome in macrophages in pathological conditions related to gout¹². Meanwhile, the mechanism of action of UA in vaccine responses may be distinct from that of inflammatory pathways, as seen in unchanging antigen-specific antibody levels during vaccination with AV in Casp1 and ASC knockout mice compared to the wild-type¹⁰. Additionally, the SE adjuvant MF59 can elicit adjuvanticity independent of the Nlrp3 inflammasome but requiring MyD88 for an antibody response⁹. Thus, UA-mediated inflammasome activation may not be responsible for stimulating antibody responses during SE-adjuvant vaccination. According

to our experimental results, MSU potentiated DC antigen presentation. Through the transcriptomic data, we presume that the various pathways besides the NLRP3 inflammasome pathway are involved in DC activation, and that the utmost increase in TNF- α signaling via NF- κ B may be crucial for the MSU stimulation in DCs. We also propose a direct influence of MSU on B cells, showing transcriptional changes in typical B cell activation processes needed for vaccine responses, such as B cell proliferation, cellular responses to cytokine signaling, and the IL-2 signaling pathway. However, current suggestions regarding the intracellular mechanisms are based on transcriptomic data. Therefore, further studies are required in order to identify these signaling pathways in detail.

This study demonstrates the role of UA in the innate immune responses, humoral responses, and T cell responses in the context of emulsion adjuvant effects. These results indicate that UA plays a crucial role in the adjuvanticity of AV, by inducing DC activation, recruiting innate immune cells in the early phase, and enhancing subsequent CD4 and CD8 T cell responses, as well as humoral responses. Furthermore, we could further demonstrate the influence of UA on the actual protection provided by the vaccine using HA antigen and influenza viral challenge experiments. The addition or inhibition of UA resulted in differences in survival rates and infection severity, with varying levels of antibody responses. Based on the results with the Ova antigen, we expect that the protection against influenza would be dependent on UA. However, a limitation of this study is that cellmediated protection was not verified experimentally. Further investigations should be conducted to understand how UA influences overall immune responses across various vaccine antigens and to fully comprehend variations among different antigens.

We showed that the temporal release of UA by the SE adjuvant played an essential role in immunogenicity by promoting the activation of DCs and B cells. These findings help better understand the mechanism of action of SE adjuvants by presenting the DAMP pathway as an immunogenic pathway.

Methods

Mice

Wild-type (WT) C57BL/6 (B6) and BALB/c mice (6–8 week old, female) were purchased from Orient Bio (Seongnam, South Korea). OT-I (C57BL/6-Tg(TcraTcrb)1100Mjb/J) and OT-II (B6.Cg-Tg(TcraTcrb)425Cbn/J) mice were purchased from Jackson Laboratories (ME, USA). Mice were maintained under specific pathogen-free conditions. Anesthesia and euthanasia were performed following the approved IACUC protocols. For subcutaneous injection, submandibular (facial) bleeding, and intranasal virus challenge, mice were anesthetized with isoflurane inhalation in an anesthesia jar. For tissue sampling and terminal bleeding (via cardiac puncture), mice were euthanized with exposure to CO₂. The animal experiments were approved by the Institutional Animal Care and Use Committee of Institut Pasteur Korea (IACUC approval no. IPK-20012-C2, IPK-21003-D2, and IPK-23005).

Immunization

Mice were vaccinated with single or double (prime-boost) doses of antigens and additives as described below. Immunization was performed subcutaneously at the base of the tail, in less than 150 μL of inoculum. For the immunization, we used following materials: endotoxin-free ovalbumin (Ova) (10 $\mu g/mouse$ for primary and 50 $\mu g/mouse$ for secondary immunization, Worthington, OH, USA), influenza A/Puerto Rico/8/1934(H1N1) (PR8) hemagglutinin (HA) protein (0.1 or 0.5 $\mu g/mouse$, SinoBiological, China), AV (50 $\mu L/mouse$, Invivogen, CA, USA), uricase (10 unit/mouse, Sigma-Aldrich, MO, USA), febuxostat (100 $\mu g/mouse$, Sigma-Aldrich), and monosodium urate (MSU, 500 $\mu g/mouse$, Invivogen). AV was used as a preclinical grade SE adjuvant with a formulation similar to that of MF59.

Viral challenge experiments

Vaccinated mice were intranasally infected with a highly lethal dose of the PR8 virus (400 PFU, 20 \times LD $_{50}$ for a single dose and 2000 PFU, 100 \times LD $_{50}$ for a double dose vaccination model), using 20 μL of inoculum per mouse,

administered by placing droplets on the nostrils and allowing inhalation of the solution. After infection, the mouse body weight was monitored daily for 14 days, and the mice were euthanized at the humane endpoint. The humane endpoint was determined based on a scoring system measuring body weight loss, physical appearance, and behaviors. Since the infected mice with > 25% weight loss typically reached score of endpoint by revealing anorexia, progressive dehydration, and reduced mobility, this was the final criterion for scoring death and performing euthanasia.

DAMP assays

Serum and inguinal LN samples were collected at the indicated time points. For serum separation, blood samples were clotted for 1 h at 4 °C and centrifuged at $10,000 \times g$ at 4 °C for 10 min. To prepare LN fluids without rupturing cells, two inguinal LNs from each mouse were dissociated into a single-cell suspension by grinding them on a 70 μ m cell strainer in 300 μ l of PBS. Supernatants were collected by centrifugation at 300 $\times g$ for 10 min at 4 °C. DAMP assays were performed using UA and ATP assay kits (Abcam, Cambridge, UK), and a Quanti-iT PicoGreen dsDNA assay kit (Thermo Fisher Scientific, MA, USA) according to the manufacturer's protocol.

Flow cytometry

Flow cytometry was performed to detect cell surface proteins and intracellular cytokines in single-cell suspensions of various tissues and immune cells. Single-cell suspensions were prepared by dissociating the tissues through a 70 µm cell strainer. For the preparation of innate immune cells, tissues were treated with collagenase type IV (Worthington, 400 U/tissue) at 37 °C (30 min for the spleen, 15 min for LNs) prior to passing through the cell strainer. The following antibodies were purchased from BD Biosciences (NJ, USA) for detection of each molecules: CD8 (53-6.7), CD4 (RM4-5), CD95 (Jo2), CD279 (PD-1) (J43), CD185 (CXCR5) (2G8), CD80 (16-10A1), NK1.1 (PK136), CD317 (PDCA-1) (927), CD11b (M1/70), Siglec-F (E50-2440), and CD69 (H1.2F3). The following antibodies were purchased from Biolegend for detection of each molecules: CD62L (MEL-14), CD19 (6D5), GL7 (GL7), CD3 (17A2), Ly6G (1A8), Ly6C (HK1.4), CD86 (GL1), CD11c (N418), F4/80 (BM8), MHC II (I-A/I-E) (M5/114.15.2), IL-2 (JES6-5H4), TNF (MP6-XT22), IFN-γ (XMG1.2), and CD185 (CXCR5) (L138D7). Staining was performed with a mouse Fc block (BD Biosciences). The H2Kb-SIIN-FEKL reagent was provided by the NIH Tetramer Core Facility (GA, USA). To assess cell viability, we used the following viability kits prior to staining: Zombie Aqua or Zombie NIR (BioLegend). For intracellular cytokine staining, the Cytofix/Cytoperm solution kit (BD Biosciences) was used according to the manufacturer's protocol. Stained cells were analyzed using CytoFLEX LX (Beckman Coulter, Brea, CA, USA), and the data were analyzed using FlowJo software (BD Biosciences).

Bead-based cytokine array and cytokine ELISA

Mouse inflammatory cytokine levels in LN fluid and serum were analyzed using bead-based cytokine assays (LEGENDplex mouse inflammation panel, BioLegend), according to the manufacturer's instructions. LN fluids were used for the cytokine array without dilution, and serum samples were 1:1 diluted with the assay buffer. All samples were analyzed using CytoFLEX LX (Beckman Coulter). Mouse IL-18 and CXCL10 levels were determined using DuoSet ELISA kits (R&D systems).

Antibody ELISA

Antigen-specific immunoglobulin (Ig) levels were determined by ELISA, as described previously 40 using 96-well EIA/RIA high-binding plate (Corning, NY, USA) coated with Ova (2 μ g/mL in PBS, Worthington) or HA (2 μ g/mL in PBS, SinoBiological). We used the following antibodies conjugated with horseradish peroxidase (HRP): goat anti-mouse IgM, goat anti-mouse IgG, goat anti-mouse IgG1, goat anti-mouse IgG2b, and goat anti-mouse IgG2c (all from Southern Biotech, AL, USA). HRP activity was measured using the BD OptEIA Reagent Set (BD Biosciences) and stopped using 2 N H₂SO₄.

Plague reduction neutralization test (PRNT)

Mouse sera were serially diluted in infection media (DMEM supplemented with 0.3% BSA and 2 $\mu g/mL$ TPCK-treated trypsin). Each diluted sample was mixed with an equal volume of virus suspension (100 pfu/well) and incubated at room temperature for 1 h. MDCK cells were cultured to confluence in 12-well cell culture plates 24–36 h before the experiment, washed with PBS, and infected with each serum-virus mixtures at 37 °C for 1 h. After incubation, the mixtures were removed, and the cells were overlaid with agarose media (0.5% agarose, DMEM with 0.3% BSA and 2 $\mu g/mL$ TPCK-treated trypsin at final concentration). The plates were incubated at 37 °C with 5% CO $_2$ for 48 h. Following incubation, the cells were fixed with 4% paraformaldehyde at room temperature for at least 15 min before removing the agarose overlay. The fixed cells were then stained with 0.1% crystal violet, and washed with water. Plaques were counted after the plates were dried. PRNT $_{50}$ titers were calculated as the reciprocal of the lowest serum dilution at which 50% of the virus was neutralized compared to the infection control (with no serum).

Intracellular cytokine staining

Cells from the LNs and spleens were stimulated with Ova peptides in media at 37 °C for 5 h in the presence of the protein transport inhibitors GolgiStop and GolgiPlug (BD Biosciences), in 96-well cell culture plates (1×10^6 cells/well). We used a mixture of Ova MHC class I peptide epitope (OVA 257–264, Invivogen) and the Ova MHC class II epitope (OVA 323–339, Invivogen). The cells were subjected to cell surface and intracellular cytokine staining.

Generation of bone marrow-derived dendritic cells (BMDCs) and macrophages (BMMs)

BMDCs and BMMs were prepared by culturing B6 female mouse bone marrow cells in RPMI-1640 (Welgene, South Korea) supplemented with 10% heat-inactivated fetal bovine serum (Gibco), 10 mM HEPES (Welgene), 100 U/mL penicillin and 100 µg/mL streptomycin (Welgene), and 50 µM β -mercaptomethanol (Sigma-Aldrich), supplemented with 2 mM L-glutamine (Welgene) for BMDCs and 2 mM sodium pyruvate (Welgene) for BMMs. Cell cultures were supplemented with 20 ng/mL GM-CSF for BMDC differentiation or 20 ng/mL M-CSF for BMM differentiation (Miltenyi Biotec, Germany). BMDCs were harvested by collecting non-adherent cells on day 10. BMMs were harvested on day 6 by collecting adherent cells using trypsinization.

DC-T cell proliferation assay

The antigen presentation capacity of the DCs was evaluated by T cell proliferation after DC-T cell co-culture. BMDCs were stimulated with Ova (80 $\mu g/mL)$, Ova + MSU (100 $\mu g/mL)$ or Ova + MSU (300 $\mu g/mL)$ for 20 hin 96-well round-bottom cell culture plates (SPL Life Sciences, Pocheon, South Korea). For DC recovery from the MSU culture, we isolated CD11c⁺ cells using anti-CD11c magnetic beads (Mojosort nanobeads, BioLegend) and a magnet (Easysep magnet, STEMCELL Technology, Vancouver, Canada). To isolate OT-I or OT-II cells, we obtained the spleen and LNs from each mouse and enriched the naïve OT-I or OT-II cells by negative selection using a mouse pan-naïve T cell isolation kit (EasySep, STEMCELL Technology). To track the proliferation of T cells, we stained the isolated T cells with 0.5 μM CFSE (CellTrace cell proliferation kit, Invitrogen, MA, USA) at 37 °C for 5 min, followed by quenching on ice for 5 min. A mixture of DCs and CFSE-labeled T cells was incubated for 3 days, and CFSE dilutions were measured by flow cytometry. The ratios of cell number between the DCs and T cells were 1:1, 1:5, and 1:10. T-cell CFSE levels were measured on days 0 and 3.

Stimulation of immune cells with MSU

BMDCs and BMMs were cultured from WT B6 mouse bone marrow cells, as described above. Splenic B and T cells were isolated using an EaspSep mouse B cell isolation kit and a pan-naïve T cell isolation kit (STEMCELL Technology). BMDCs (5×10^5 cells/well) in 24-well non-TC cell culture plates (Nunc, Roskilde, Denmark), BMMs (5×10^5 cells/well), splenic B (5×10^5 cells/well), and T cells (2×10^5 cells/well) in 24-well cell culture

plates (SPL Life Sciences) were stimulated with MSU as indicated, either with or without 100 ng/mL LPS priming. Activation marker expression levels were analyzed after stimulation with 100 or 300 μ g/mL MSU for 24 h, by flow cytometry. RNA sequencing was performed after stimulation with 300 μ g/mL MSU for 3 h.

RNA sequencing and data analysis

Total RNA was extracted using the TRIzol reagent (Thermo Fisher Scientific) according to the manufacturer's protocol. The RNA amount was quantified using nanodrop (Thermo Fisher Scientific), and $\geq 2 \mu g$ RNA per sample was used for RNA sequencing.

RNA sequencing was performed by ROKIT Genomics (South Korea). For the analysis of the bulk RNA sequencing data, we used the mouse genome (mm10_NCBI_108)⁴¹ along with gene annotations from mm10.refGene.gtf⁴². We employed Hisat2 v2.1.0⁴³ for mapping and alignment, and featureCounts v2.0.3 for counting⁴⁴. After each step, we conducted quality control checks using FastQC 0.11.9 and MultiQC v1.12^{45,46}. To identify differentially expressed genes (DEGs), raw counts were obtained from the sequencing data. Genes with zero counts across all of the samples were removed. We then searched for unusual values or outliers using Cook's distance from the DESeq2 1.40.2 package⁴⁷ and the Molecular Degree Perturbation (MDP) score from the mdp 1.24.0 package in R⁴⁸. For the actual differential expression analysis, we used the default parameters of the DESeq2 package⁴⁷. We considered genes with padj < 0.01 and | log2FC | > 1 as statistically significant DEGs.

For functional enrichment analysis, we selected DEGs using a statistical cutoff of a padj <0.05 and $\left|\log 2FC\right|>1$. We ranked these DEGs by log2FC and conducted a pre-ranked gene set enrichment analysis (GSEA) using the fgsea 1.28.0 package⁴⁹. Comprehensive annotation datasets were used, including "BioCarta 2016," "BioPlanet 2019," "GO Biological Process 2021," and others $^{50-57}$. To ensure robust and relevant pathways, we excluded those with sizes <15 or >500 during enrichment analysis. We considered pathways with padj <0.05 as statistically significant. The analyses were performed using the fgsea and hypeR 2.0.1 packages in R software 49,58 .

Statistical analysis

All statistical analyses were performed using Prism 9 software (GraphPad Software, CA, USA). Normal distribution was evaluated using the Shapiro-Wilk test before determining statistical significance (normal distribution if p > 0.01). Equality of variance was also examined with the Brown-Forsythe test for more than three groups and with the F-test for comparison of two groups. For comparison of the three groups, statistical significance was determined by one-way ANOVA, Welch ANOVA, or the Kruskal-Wallis test, depending on the normal distribution and variance equality, followed by multiple comparison tests using the two-stage linear step-up procedure of Benjamini, Krieger, and Yekutieli. For comparison of data between the two groups (AV vs. AV+febuxostat), we used the Mann-Whitney U test, unpaired t-test, or Welch's t-test, depending on normal distribution and variance equality. Survival data were analyzed using the log-rank test. Statistical significance is indicated by P values (*P < 0.05, **P < 0.01, ***P < 0.001, ***P < 0.001).

Data availability

The RNA sequencing datasets generated and analysed during the current study are available in the Gene Expression Omnibus repository (accession number GSE273800). All other data supporting the findings of this study are available within the article and its Supplementary Information file.

Received: 27 November 2024; Accepted: 7 April 2025; Published online: 16 April 2025

References

 Marichal, T. et al. DNA released from dying host cells mediates aluminum adjuvant activity. Nat. Med. 17, 996–1002 (2011).

- McKee, A. S. et al. Host DNA released in response to aluminum adjuvant enhances MHC class II-mediated antigen presentation and prolongs CD4 T-cell interactions with dendritic cells. *Proc. Natl. Acad.* Sci. USA 110, E1122–E1131 (2013).
- Kool, M. et al. Alum adjuvant boosts adaptive immunity by inducing uric acid and activating inflammatory dendritic cells. J. Exp. Med. 205, 869–882 (2008).
- 4. Riteau, N. et al. ATP release and purinergic signaling: a common pathway for particle-mediated inflammasome activation. *Cell Death Dis.* **3**, e403 (2012).
- Detienne, S. et al. Central role of CD169(+) lymph node resident macrophages in the adjuvanticity of the QS-21 component of AS01. Sci. Rep. 6, 39475 (2016).
- Seubert, A., Monaci, E., Pizza, M., O'Hagan, D. T. & Wack, A. The adjuvants aluminum hydroxide and MF59 induce monocyte and granulocyte chemoattractants and enhance monocyte differentiation toward dendritic cells. *J. Immunol.* 180, 5402–5412 (2008).
- Calabro, S. et al. Vaccine adjuvants alum and MF59 induce rapid recruitment of neutrophils and monocytes that participate in antigen transport to draining lymph nodes. *Vaccine* 29, 1812–1823 (2011).
- Cioncada, R. et al. Vaccine adjuvant MF59 promotes the intranodal differentiation of antigen-loaded and activated monocyte-derived dendritic cells. PLoS ONE12, e0185843 (2017).
- Seubert, A. et al. Adjuvanticity of the oil-in-water emulsion MF59 is independent of Nlrp3 inflammasome but requires the adaptor protein MyD88. Proc. Natl. Acad. Sci. USA 108, 11169–11174 (2011).
- Kim, E. H. et al. Squalene emulsion-based vaccine adjuvants stimulate CD8 T cell, but not antibody responses, through a RIPK3dependent pathway. *Elife* 9, e52687 (2020).
- Vono, M. et al. The adjuvant MF59 induces ATP release from muscle that potentiates response to vaccination. *Proc. Natl, Acad. Sci. USA* 110, 21095–21100 (2013).
- Martinon, F., Petrilli, V., Mayor, A., Tardivel, A. & Tschopp, J. Goutassociated uric acid crystals activate the NALP3 inflammasome. *Nature* 440, 237–241 (2006).
- Yoshimura, S., Bondeson, J., Foxwell, B. M., Brennan, F. M. & Feldmann, M. Effective antigen presentation by dendritic cells is NFkappaB dependent: coordinate regulation of MHC, co-stimulatory molecules and cytokines. *Int. Immunol.* 13, 675–683 (2001).
- Olguin-Alor, R. et al. A Key Role for Inhibins in Dendritic Cell Maturation and Function. PLoS ONE11, e0167813 (2016).
- Sarraf, T. R. & Sen, M. Wnt5A signaling supports antigen processing and CD8 T cell activation. Front. Immunol. 13, 960060 (2022).
- MartIn-Fontecha, A. et al. Regulation of dendritic cell migration to the draining lymph node: impact on T lymphocyte traffic and priming. *J. Exp. Med.* 198, 615–621 (2003).
- Ohl, L. et al. CCR7 governs skin dendritic cell migration under inflammatory and steady-state conditions. *Immunity* 21, 279–288 (2004).
- Hintzen, G. et al. Induction of tolerance to innocuous inhaled antigen relies on a CCR7-dependent dendritic cell-mediated antigen transport to the bronchial lymph node. *J. Immunol.* 177, 7346–7354 (2006).
- 19. Ge, S. X., Jung, D. & Yao, R. ShinyGO: a graphical gene-set enrichment tool for animals and plants. *Bioinformatics* **36**, 2628–2629 (2020).
- Hipp, N. et al. IL-2 imprints human naive B cell fate towards plasma cell through ERK/ELK1-mediated BACH2 repression. *Nat. Commun.* 8, 1443 (2017).
- Habib, T. et al. Myc stimulates B lymphocyte differentiation and amplifies calcium signaling. J. Cell. Biol. 179, 717–731 (2007).
- Heng, T. S., Painter, M. W. & Immunological Genome Project, C. The Immunological Genome Project: networks of gene expression in immune cells. *Nat. Immunol.* 9, 1091–1094 (2008).
- Heine, G. et al. Autocrine IL-10 promotes human B-cell differentiation into IgM- or IgG-secreting plasmablasts. *Eur. J. Immunol.* 44, 1615–1621 (2014).

- Ottens, K. & Satterthwaite, A. B. IRF4 has a unique role in early b cell development and acts prior to CD21 expression to control marginal Zone B Cell Numbers. Front. Immunol. 12, 779085 (2021).
- 25. Dahlgren, M. W. et al. Type I Interferons promote germinal centers through B cell intrinsic signaling and dendritic cell dependent Th1 and Tfh Cell Lineages. *Front. Immunol.* **13**, 932388 (2022).
- Syedbasha, M. et al. Interferon-lambda enhances the differentiation of Naive B cells into plasmablasts via the mTORC1 Pathway. *Cell Rep.* 33, 108211 (2020).
- Shi, Y., Evans, J. E. & Rock, K. L. Molecular identification of a danger signal that alerts the immune system to dying cells. *Nature* 425, 516–521 (2003).
- Phan, A. T. et al. The type I IFN-IL-27 axis promotes mRNA vaccine-induced CD8 (+) T cell responses. bioRxiv https://doi.org/10.1101/2025.01.16.633383 (2025).
- Mascanfroni, I. D. et al. IL-27 acts on DCs to suppress the T cell response and autoimmunity by inducing expression of the immunoregulatory molecule CD39. Nat. Immunol. 14, 1054–1063 (2013).
- van Gisbergen, K. P., Sanchez-Hernandez, M., Geijtenbeek, T. B. & van Kooyk, Y. Neutrophils mediate immune modulation of dendritic cells through glycosylation-dependent interactions between Mac-1 and DC-SIGN. J. Exp. Med. 201, 1281–1292 (2005).
- Kobayashi, T., Kouzaki, H. & Kita, H. Human eosinophils recognize endogenous danger signal crystalline uric acid and produce proinflammatory cytokines mediated by autocrine ATP. *J. Immunol.* 184, 6350–6358 (2010).
- 32. Wang, H. B. & Weller, P. F. Pivotal advance: eosinophils mediate early alum adjuvant-elicited B cell priming and IgM production. *J. Leukoc. Biol.* **83**, 817–821 (2008).
- 33. Jaime-Sanchez, P. et al. Cell death induced by cytotoxic CD8(+) T cells is immunogenic and primes caspase-3-dependent spread immunity against endogenous tumor antigens. *J. Immunother. Cancer* **8**, e000528 (2020).
- Apetoh, L. et al. Toll-like receptor 4-dependent contribution of the immune system to anticancer chemotherapy and radiotherapy. *Nat. Med.* 13, 1050–1059 (2007).
- Ng, G. et al. Receptor-independent, direct membrane binding leads to cell-surface lipid sorting and Syk kinase activation in dendritic cells. *Immunity* 29, 807–818 (2008).
- Martinez-Reyes, C. P. et al. Uric acid has direct proinflammatory effects on human macrophages by increasing proinflammatory mediators and bacterial phagocytosis probably via URAT1. Biomolecules 10, 576 (2020).
- Neumann, K. et al. Clec12a is an inhibitory receptor for uric acid crystals that regulates inflammation in response to cell death. *Immunity* 40, 389–399 (2014).
- Li, K. et al. The uric acid crystal receptor Clec12A potentiates type I interferon responses. Proc. Natl Acad. Sci. USA 116, 18544–18549 (2019).
- 39. Braga, T. T. et al. Sensing soluble uric acid by Naip1-Nlrp3 platform. *Cell Death Dis.* **12**, 158 (2021).
- Kim, D. B. et al. In planta production and validation of neuraminidase derived from genotype 4 reassortant eurasian Avian-like H1N1 virus as a vaccine candidate. *Plants* 11, 2984 (2022).
- National Library of Medicine, National Center for Biotechnology Information https://www.ncbi.nlm.nih.gov/genome/annotation_euk/ Mus_musculus/108/.
- UCSC Genome Browser https://hgdownload.soe.ucsc.edu/ goldenPath/mm10/bigZips/genes/.
- Kim, D., Langmead, B. & Salzberg, S. L. HISAT: a fast spliced aligner with low memory requirements. *Nat. Methods* 12, 357–360 (2015).
- Liao, Y., Smyth, G. K. & Shi, W. featureCounts: an efficient general purpose program for assigning sequence reads to genomic features. *Bioinformatics* 30, 923–930 (2014).
- 45. Babraham Bioinformatics http://www.bioinformatics.babraham.ac.uk/projects/fastqc/.

- Ewels, P., Magnusson, M., Lundin, S. & Kaller, M. MultiQC: summarize analysis results for multiple tools and samples in a single report. *Bioinformatics* 32, 3047–3048 (2016).
- Love, M. I., Huber, W. & Anders, S. Moderated estimation of fold change and dispersion for RNA-seq data with DESeq2. *Genome Biol.* 15, 550 (2014).
- Goncalves, A. N. A. et al. Assessing the Impact of Sample Heterogeneity on Transcriptome Analysis of Human Diseases Using MDP Webtool. *Front. Genet.* 10, 971 (2019).
- 49. Korotkevich, G. et al. Fast gene set enrichment analysis. *bioRxiv* 060012; https://doi.org/10.1101/060012 (2021).
- Nishimura, D. BioCarta. Biotech. Softw. Internet Rep. 2, 117–120 (2001).
- Huang, R. et al. The NCATS BioPlanet An Integrated Platform for Exploring the Universe of Cellular Signaling Pathways for Toxicology, Systems Biology, and Chemical Genomics. Front. Pharmacol. 10, 445 (2019).
- Gene Ontology, C. The gene ontology project in 2008. Nucleic Acids Res. 36, D440-D444 (2008).
- Gene Ontology, C. The gene ontology resource: enriching a GOld mine. *Nucleic Acids Res.* 49, D325–D334 (2021).
- 54. Martens, M. et al. WikiPathways: connecting communities. *Nucleic Acids Res.* **49**, D613–D621 (2021).
- Kanehisa, M. & Goto, S. KEGG: kyoto encyclopedia of genes and genomes. *Nucleic Acids Res.* 28, 27–30 (2000).
- Baldarelli, R. M. et al. The mouse Gene Expression Database (GXD):
 2021 update. Nucleic Acids Res. 49, D924–D931 (2021).
- Thomas, P. D. et al. PANTHER: a library of protein families and subfamilies indexed by function. *Genome Res.* 13, 2129–2141 (2003).
- 58. Federico, A. & Monti, S. hypeR: an R package for geneset enrichment workflows. *Bioinformatics* **36**, 1307–1308 (2020).

Acknowledgements

We thank the NIH Tetramer Core Facility (contract number 75N93020D00005) for providing H2K $^{\rm b}$ -SIINFEKL tetramers. This research was supported by the National Research Foundation of Korea (NRF) grants funded by the Korea government (MSIT; grant number NRF-2021R1C1C1012962 and RS-2024-00398073). The funder played no role in study design, data collection, analysis and interpretation of data, or the writing of this manuscript.

Author contributions

Conceptualization: E.H.K.; Methodology: S.M.L., K.K., and E.H.K.; Investigation: S.M.L., J.L., D.K., and E.H.K.; Data analysis: S.M.L., J.P.A., H.N., and E.H.K.; Funding acquisition: E.H.K.; Supervision: E.H.K.; Writing — original draft preparation: S.M.L. and E.H.K.; Writing — review and editing: J.L., H.N., K.K., and E.H.K.; All authors reviewed the manuscript.

Competing interests

The authors declare no competing interests.

Additional information

Supplementary information The online version contains supplementary material available at https://doi.org/10.1038/s41541-025-01130-z.

Correspondence and requests for materials should be addressed to Eui Ho Kim.

Reprints and permissions information is available at http://www.nature.com/reprints

Publisher's note Springer Nature remains neutral with regard to jurisdictional claims in published maps and institutional affiliations.

Open Access This article is licensed under a Creative Commons Attribution-NonCommercial-NoDerivatives 4.0 International License, which permits any non-commercial use, sharing, distribution and reproduction in any medium or format, as long as you give appropriate credit to the original author(s) and the source, provide a link to the Creative Commons licence, and indicate if you modified the licensed material. You do not have permission under this licence to share adapted material derived from this article or parts of it. The images or other third party material in this article are included in the article's Creative Commons licence, unless indicated otherwise in a credit line to the material. If material is not included in the article's Creative Commons licence and your intended use is not permitted by statutory regulation or exceeds the permitted use, you will need to obtain permission directly from the copyright holder. To view a copy of this licence, visit http://creativecommons.org/licenses/by-nc-nd/4.0/.

© The Author(s) 2025